

Pickup Ion Injection and Acceleration at Perpendicular Shocks

G.P. Zank¹ and A.S. Lipatov²

¹*Bartol Research Institute, University of Delaware, Newark, DE 19716, USA*

²*Max-Planck-Institut für Aeronomie, Katlenburg-Lindau, Germany*

Abstract

Results from a multiscale hybrid kinetic simulation of low plasma beta supercritical perpendicular shocks are presented. Freshly ionized pickup ions are included self-consistently. It is found that perpendicular shocks can accelerate pickup ions from an initial “thermal” shell distribution to high energies. The mechanism by which the pickup ions are energized is that of multiply reflected ion (MRI) acceleration [Zank *et al.*, 1996; Lee *et al.*, 1996]. The injection efficiency is found to be very high and maximum energies of nearly 0.5 MeV are attained. MRI acceleration may provide a solution to the so-called injection problem for anomalous cosmic rays.

1 Introduction:

Accelerated pickup ions (PIs) have been observed directly, for example, by Ulysses at a weak corotating shock [Gloeckler *et al.*, 1994]. Both pickup H^+ and He^+ were observed by the SWICS instrument to possess very hard power law spectra which extend directly out of the expected pickup ion distribution, to energies well in excess of the characteristic pickup ion cutoff velocity $v = 2u_{SW}$ (in the spacecraft frame). Here v denotes particle velocity and u_{SW} the solar wind flow velocity. It was observed too that $\sim 43\%$ of the pickup protons H^+ and $\sim 16\%$ of the He^+ was accelerated by the shock. Both the hardness of the pickup ion spectrum and the favouring of light ion acceleration over heavy ions are quite inconsistent with the expectations of diffusive/first-order Fermi shock acceleration. These results pose a challenge for models of particle acceleration at shock waves.

Besides diffusive shock acceleration, two alternatives for accelerating pickup ions at weak quasi-perpendicular shocks are shock drift acceleration [Decker, 1988] and Multiply Reflected Ion (MRI) acceleration or shock surfing [Zank *et al.*, 1996; Lee *et al.*, 1996]. Both approaches directly accelerate particles out of the pickup ion “thermal” pool. However, the MRI mechanism is found to produce high energies for pickup ions, a very flat spectrum and to have an injection efficiency which decreases with increasing particle mass. Present models of MRI acceleration treat the pickup ions as test particles and use non-selfconsistent electromagnetic fields.

Particle acceleration of PIs by the multiple reflection mechanism (or surfing) of PIs at a shock ramp is explained easily. On the PI shell distribution in the shock frame, a fraction of the PI population has so little kinetic energy, that they can be reflected by the the shock electrostatic potential jump inside the ramp. This population of ions then drifts along the shock front surface, being multiply

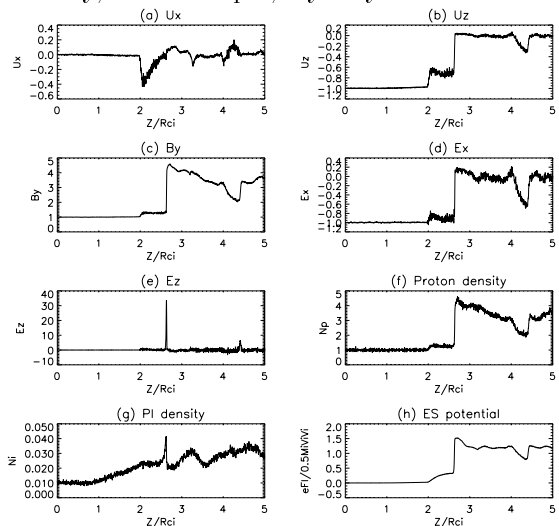


Figure 1: Profiles of the bulk velocity components u_x and u_z , the magnetic field component B_y , the electric components E_x and E_z , the proton n_p and PI n_{PI} densities, and electrostatic potential $e\phi/Mu_0^2/2$.

reflected at the shock ramp, trapped by the upstream particle Lorentz force and the electrostatic potential jump. The time spent upstream of the shock determines the maximum energy gain for a trapped PI, and results from a balance between the particle Lorentz force and the gradient of the electrostatic potential.

Unfortunately, selfconsistent kinetic simulations of quasi-perpendicular shocks, which may include PIs [Liewer *et al.*, 1995; Giacalone *et al.*, 1994], have yet to demonstrate any significant acceleration of solar wind protons and PIs by MRI-like processes in the absence of either strong wave generation or externally imposed high levels of MHD turbulence.

Shock simulations that exhibit significant MRI energization of PIs at the shock ramp are presented here. The results were obtained by using a one-dimensional, (1+2/2)D hybrid kinetic electromagnetic code (for ions and protons, we use a kinetic/particle description while for finite mass electrons, the hydrodynamical equations (electron pressure equation) is used) [Galeev *et al.*, 1991]. Anomalous resistivity and electron inertia terms are included in the code. Although we assume spatial variation along the z direction only, all three components of the electromagnetic fields and particle velocities are retained. The shocks studied have upstream parameters, which are expected of the solar wind in the transition layer of the termination shock and are all quasi-perpendicular ($\theta_{Bn} = 90^\circ, 72^\circ$). The initial proton and PI velocity distribution functions are Maxwellian shell respectively, the latter of which is assumed to have been thickened.

The bulk velocity of solar wind protons and PIs is equal initially, $\mathbf{u}_{PI} = \mathbf{u}_0$. There are 4097 – 8193 cells in z , and initially 512,000 macroprotons and 512,000 macroions. Plasma is injected continuously into the left of the simulation box and the shock is formed by reflecting the plasma off the right-hand end of the box. The simulation time step is $5 \times 10^{-5} T_{ci}$, where $T_{ci} = 2\pi/\Omega_i$ and Ω_i is the proton gyrofrequency. Such small spatial and time scales were chosen to resolve the ramp on an electron inertial length scale and to provide an accurate calculation of PI trajectories as they

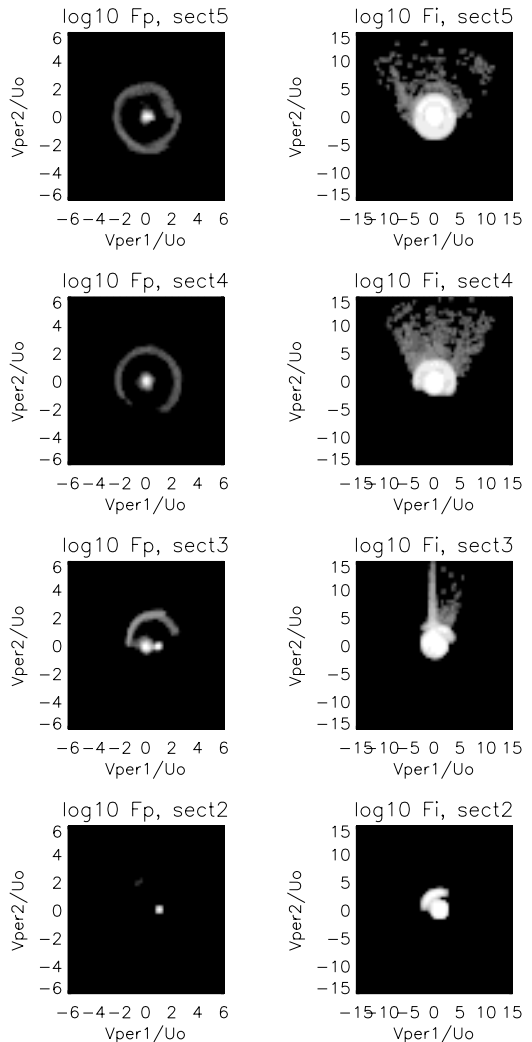


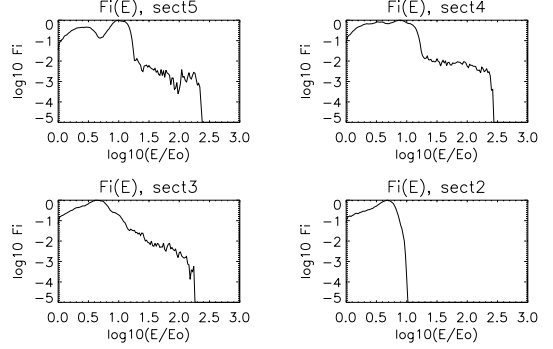
Figure 2: The projection of the protons (left column) and H^+ PI (right column) distribution onto the velocity plane for spatial sections ranging from downstream to upstream. Here $v_{\perp 1} \parallel \mathbf{v}_z$ and $v_{\perp 2} \parallel \mathbf{v}_x$ are the velocity components perpendicular to the magnetic field. they are transmitted across the ramp.

2 Results

Figure 1 illustrates a shock simulation with $M_A = 5$, $n_{PI}/n_0 = 0.01$, and resistive diffusion length $l_d = 0.006c/\omega_{pi}$ at time $t = 3.8T_{ci}$. Only half the simulation box is shown. The velocity, magnetic field, density, and electron pressure are normalized to the upstream velocity, magnetic field, proton density, electron pressure, and the electric field and electrostatic potential to the upstream motional

electric field $u_0 B_0/c$ and incoming proton kinetic energy $Mu_0^2/2$. The formation of a shock transition layer with a strong foot in the PI density profile (g) and a thin ramp, $\Delta_{ramp}/r_{ci} < 0.05$ in the magnetic field and electrostatic potential profiles (Figures 1c and 1h) is evident. An additional jump forms at a distance $\delta z \approx 0.6r_{ci}$ before the ramp in the electromagnetic field, bulk velocity and proton density profiles. The peak in PI density corresponds to temporarily trapped and accelerated PIs (Figure 1g).

Figure 2 shows $v_{\perp 2}$ vs $v_{\perp 1}$ for the protons and H^+ PIs at different locations relative to the shock ramp, where $v_{\perp 1}$ and $v_{\perp 2}$ are the velocity components, perpendicular to the magnetic field. The panels of Figure 2 are arranged in ascending order from the bottom according to position as follows: far upstream (bottom panel), on the shock front, just downstream of the shock, and, the top panel, far downstream. The left (right) column gives the projected proton (PI) distribution. The proton distribution function has a supersonic core ahead of the ramp and a downstream subsonic core. Reflected protons are present ahead of the ramp, while the downstream transmitted protons



form a halo due to phase mixing. The bottom right panel shows a typical distribution which results from ion reflection at a perpendicular shock. Such distributions are seen at virtually all quasi-perpendicular shocks, both observationally (e.g., *Scopke*, 1995) and in simulations (e.g., *Leroy*, 1982) and contribute essentially to the formation of the ion shock foot. If the number and energy density of the reflected PIs were sufficiently high at the termination shock, the foot structure and length scales would be determined primarily by reflected PIs rather than the colder more numerous solar wind protons [*Zank et al.*, 1996; *Liewer et al.*, 1995]. The second panel from the bottom shows the PI distribution at the shock ramp and a strong transverse acceleration of PIs along the shock front is evident with the formation of an extended “tongue” along $v_{\perp 2}$. Finally, phase mixing occurs far downstream.

Figure 3 illustrates the energy spectrum of accelerated H^+ PIs for spatial sections ranging from downstream to upstream. The PI energy spectrum has two parts, as discussed by *Zank et al.* [1996]; a shell-like distribution with an energy cut-off at about $E_0 = M_{PI}u_0^2/2$ in the solar wind frame and an accelerated PI component which emerges from the shell distribution as a hard/flat power law spectrum. The accelerated PI energy spectrum may be approximated by the power law $F_i \propto dN/N \sim (E/E_0)^{-k}$, where the energy E is calculated in the solar wind frame and N denotes the PI number density. In the present case, the index k is about 1.0-1.3 inside a vicinity of ramp. The similarity between the spectra produced by the hybrid simulation here, a test particle-mesh simulation [*Lipatov et al.*, 1998] and those obtained from the quasi-analytical approach of *Zank et al.* [1996] is close. The spectrum produced by the MRI mechanism is much harder than expected of diffusive shock acceleration, which would produce an $\sim E^{-2}$ spectrum for the shock compression ratio used here. Also, as discussed in §2 of *Zank et al.* [1996], diffusive shock acceleration at a perpendicular shock imposes severe energy constraints on the particles to be accelerated, constraints which are absent for MRI acceleration. The maximum transverse energy of accelerated PIs ($\log_{10} E_{max}/E_0 = 2.3 - 2.5$) is higher than estimated by *Zank et al.* for a ramp thickness of $L_{ramp} < 0.05r_{ci}$. The simulation with a high PI density ($n_{PI}/n_0 = 0.1$) is less efficient at accelerating PIs ($\log_{10} E_{max}/E_0 = 1.7$) thanks to the formation of a strong foot and a decrease in the electrostatic potential jump. In the simulation with large resistive diffusion length $l_d = 0.25c/\omega_{pi}$, the maximum energy of accelerated PIs decreases significantly since the ramp thickness is too large, and MRI acceleration becomes ineffective. For

Figure 3: The energy spectrum of accelerated H^+ PIs for spatial sections ranging from downstream to upstream.

the simulation with small resistive diffusion length, $l_d = 0.001c/\omega_{pi}$, the electrostatic jump at the ramp is comparable with the fluctuation level and no significant acceleration occurs. In the quasi-perpendicular case, $\theta_{BN} = 72^\circ$, the formation of a whistler precursor decreases the efficacy of PI acceleration.

3 Conclusions

Kinetic hybrid simulations of the acceleration of H^+ pickup ions at low solar wind proton $\beta_p \leq 0.1$ collisionless quasi-perpendicular shocks (with a low PI density ($n_{PI}/n_0 < 0.1$) and appropriate anomalous resistivity $0.006c/\omega_{pi} \leq l_d < 0.25c/\omega_{pi}$) reveal several new features, as well as providing support for the basic test-particle analysis of Zank *et al.* [1996] and Lee *et al.* [1996]. Our results may be enumerated as follows. (1) The energy spectrum of accelerated H^+ PIs at quasi-perpendicular shocks may be approximated by the power law $F_i(E) \approx (E/E_0)^{-k}$, where k varies from 1.0 to 1.3. This spectrum is a little harder than that obtained by the quasi-analytical approach, but both approaches give spectra which are considerably harder than those predicted by diffusive shock acceleration. (2) For MRI acceleration of H^+ and He^+ ions to be effective, a ramp thickness comparable to the electron inertial length scale is needed, whereas for heavy ions, it is sufficient to have a ramp thickness comparable to that of the ion inertial length. Thus, the key factor determining the efficacy of MRI acceleration is the existence of a strong steep ramp inside the shock transition layer. The simulation does not show MRI acceleration of H^+ and He^+ at shocks with $\beta_p > 0.1$. Further details can be found in Lipatov and Zank [1999].

Acknowledgements: This work has been supported in part by an NSF-DOE award ATM-9713223, an NSF award ATM-9713432, NASA grants NAG5-6469 and NAG5-7796, JPL contract 959167, and a NASA Space Grant College award NGT5-40024.

References

- Decker, R.B., 1988, *Space Sci. Rev.* **48**, 195.
Galeev, A.A., A.S. Lipatov, and A.A. Malgichev, 1991, *Sov. J. Plasma Phys.* **17**, 701.
Giacalone, J., J.R. Jokipii, and J. Kóta, 1994, *J. Geophys. Res.* **99**, 19,351.
Gloeckler, G., et al., 1994, *J. Geophys. Res.*, **99**, 17,637.
Lee, M.A., V.D. Shapiro, and R.Z. Sagdeev, 1996, *J. Geophys. Res.*, **101**, 4777.
Liewer, P.C., S. Rath, and B.E. Goldstein, 1995, *J. Geophys. Res.* **100**, 19,809.
Lipatov, A.S., G.P. Zank, and H.L. Pauls, 1998, *J. Geophys. Res.*, **103**, 29,679.
Lipatov, A.S., and G.P. Zank, 1999, *Phys. Rev. Lett.*, in press.
Sckopke, N., 1995, *Adv. Space Res.* **15**, (8/9), 261.
Zank, G.P., H.L. Pauls, I.H. Cairns and G.M. Webb, 1996, *J. Geophys. Res.*, **101**, 457.